Composites: Part A 157 (2022) 106925

Contents lists available at ScienceDirect

Composites Part A

journal homepage: www.elsevier.com/locate/compositesa

4D printing of electroactive shape-changing composite structures and their programmable behaviors

Xinyu Dong [a], Fenghua Zhang [a,*], Linlin Wang [a], Yanju Liu [b], Jinsong Leng [a,*]

[a] Centre for Composite Materials and Structures, Harbin Institute of Technology (HIT), No.2 Yikuang Street, Harbin 150080, People's Republic of China
[b] Department of Astronautic Science and Mechanics, Harbin Institute of Technology (HIT), No. 92 West Dazhi Street, Harbin 150001, People's Republic of China

ARTICLE INFO

Keywords:
A. Smart materials
A. Multifunctional composites
E. 3-D Printing

ABSTRACT

4D printing is an advanced manufacturing technology that combines the convenience of additive manufacturing and uses stimuli-responsive materials, which has great application potentials in the field of smart structures. Using electroactive shape memory polymer composites (SMPCs), smart devices with remote control capabilities without a heat source can be prepared by 4D printing. In this work, a variety of 4D printed structures based on PLA/CNT composites were fabricated by FDM. Electroactive SMPC filaments with different CNT contents were prepared, and their electrical, thermal, and shape-memory properties were investigated. Moreover, a series of 2D and 3D printed complex structures were designed and manufactured to realize their shape recovery behavior under the electrical field. The relationship between the electroactive shape-memory performance of 4D printed structures, structural design, and printing parameters was obtained. This work could provide a new feasible way for the design and manufacturing of electroactive devices in the future.

1. Introduction

In 2013, Skylar Tibbits of Massachusetts Institute of Technology (MIT) reported a new type of rope structure that could automatically bend into the word "MIT" after being immersed in water, and this phenomenon first revealed the concept of four-dimensional (4D) printing [1]. Researchers have initially defined 4D printing as "3D printing + time", (addition of the time dimension to 3D printing); thus, the shape and function of a printed structure can change with time. Currently, 4D printing usually refers to additive manufacturing using smart materials. Smart structures experience structural changes under certain external excitations [2]. Moreover, 4D printed products have strong customizability. Design ideas can be directly programmed into different structures in a modeling process, providing greater design freedom for printed products. In addition, during a design process, a complex structure can be first made into a simpler one and then transformed into the required complex geometry under external stimuli, thereby reducing the difficulty of forming [3]. Currently, 4D printed structures are generally applied to biomedicine, aerospace, photonic devices, and soft robotics [4–7].

Smart materials, such as shape memory polymers (SMPs), shape memory alloys, piezoelectric materials, liquid crystal elastomers, and electroactive polymers are used for 4D printing [8–10]. Among them, SMPs have the advantages of low cost, adjustable transition temperature, different driving methods, and large deformation [11–15]. SMPs are stimuli-responsive materials, which can be transformed into a temporary shape under an external force when heating above the transition temperature. The temporary shape can be fixed during cooling under the same external force. When SMPs are heated above the transition temperature, they can automatically recover from the temporary shape to the original shape and complete one shape memory cycle. Shape memory polymer composites (SMPCs) are composed of SMPs with other functional materials, and they easily respond to light [16,17], electricity [18–20], magnetic field [21,22] and other stimuli and have improved mechanical properties. Liu et al. [23] used polylactic acid (PLA) as the raw material to fabricate laminated Miura-origami tessellations and tubes by 4D printing and realized their shape memory process under compression. The resultant specimens manifested considerable shape memory performance with a shape recovery rate of greater than 94% and a volume change rate of 289%. Zhang et al. [24] prepared 4D printed circular braided tubes and investigated the effects of different structural parameters and temperatures on the shape memory behavior of the products. Furthermore, by introducing a silicone elastomer, the mechanical properties and shape memory properties of composites can

* Corresponding authors.
E-mail addresses: fhzhang_hit@163.com (F. Zhang), lengjs@hit.edu.cn (J. Leng).

https://doi.org/10.1016/j.compositesa.2022.106925
Received 26 September 2021; Received in revised form 4 February 2022; Accepted 11 March 2022
Available online 14 March 2022
1359-835X/

be significantly improved.

Stimuli-responsive methods have significant impacts on the application of SMPCs in different fields. Electroactive SMPCs are less dependent on environmental factors, and their shape recovery can be realized by the Joule heating effect. Electroactive SMPCs have good filling dispersion, uniform heat distribution and remote control, and a high driving efficiency [25–28]. The most commonly used matrix materials for electroactive SMPCs are epoxy [29], cyanate [30], polystyrene [31], polyurethane [32], and PLA [33]. According to their shapes, conductive fillers can be divided into zero-dimensional particles, one-dimensional fibers, and two-dimensional layers or films. In addition, fillers can be divided into two major categories- carbonaceous and metal. Generally, carbonaceous fillers include carbon nanotubes (CNTs), carbon nanofibers (CNFs), graphene, and carbon black, whereas metal fillers include gold, silver, copper, and nickel [34–36].

Numerous methods have been developed to manufacture electroactive SMPCs. Wang et al. [37] used a numerically controlled spray-evaporative deposition process to deposit CNT layers on shape memory PU films to prepare SMP/CNT composites with a regular distribution of CNTs. Zhang et al. [38] prepared a novel nanocomposite using an ultra-thin polyacrylonitrile-based electrospinning CNF film and Nafion. However, most of these methods are unsuitable for large-scale production because of their complex processes, harsh conditions, long forming cycles, and high cost. Different from the abovementioned methods, 4D printing represented by the fused deposition method (FDM) is a low-cost, fast forming process. In this process, mixed raw materials are extruded into filaments. Subsequently, these filaments are melted and deposited to form various structures [39]. However, very few reports are available on the 4D printing of electroactive SMPCs, and these reports do not elaborate on the relationship between the electrical and thermal properties of 4D printed composites and structures. Moreover, no research has revealed the main influencing factors for the electroactive shape memory performance of 4D printed structures [40–44]. Therefore, in the present work, 4D printed structures were formed based on electroactive shape memory PLA/CNT composites by FDM. The shape recovery behaviors of filaments and different 4D printed structures were recorded. Furthermore, the influence of structural design on the electroactive shape memory performance was investigated.

2. Experimental section

2.1. Fabrication of shape memory PLA/CNT composite filaments

PLA (4032D) provided by Harbin Institute of Technology was used after drying at 50 °C for four hours [44]. CNTs (TNIM4) were supplied by Chengdu Organic Chemicals Co. Ltd. After weighing PLA and CNTs in proportion, they were mixed by shaking and stirring. Subsequently, a 1.75 ± 0.05 mm electroactive PLA/CNT composite filament with uniform particle distribution was obtained through a consecutive twin-screw extruder (CTE 20, Coperion Nanjing Machinery Co., Ltd). Two types of composite filaments with different CNT ratios (5 wt% and 8 wt %) were prepared. Fig. 1 schematically presents the preparation process of electroactive PLA/CNT composite filaments.

2.2. 4D printing of composite structures

The FDM was used to realize the 4D printing of smart structures. A GeeeTech I3 Pro C printer and a standard nozzle of 0.4 mm diameter were used for 4D printing. In order to ensure a smooth extrusion of the nozzle, the printing temperature and the hotbed temperature were set to 200 °C and 45 °C, respectively; thus, printed structures remained firmly attached to the hotbed. The linear filling method was adopted, and the filling rate was set to 100% to ensure internal continuity. The height of a single layer was set to 0.2 mm (half of the nozzle diameter) to obtain better printing quality.

2.3. Characterization

2.3.1. Electrical property measurement

Composites with high electrical properties generally manifest better electroactive shape recovery behavior. Good and uniform conductivity ensures a faster response speed and more uniform recovery. The electrical properties of the composite filaments were tested based on the law of resistance [45].

$$R = \rho \frac{l}{S} \tag{1}$$

where ρ is the resistivity of the specimen of uniform shape, R is the electrical resistance, S is the cross-sectional area, and L is the length of the specimen.

Electrical property measurements were carried out through the following steps. (1) Each composite filament was cut into small specimens at different positions to keep them straight and reflect the uniformity of the composite filament. (2) The average cross-sectional area, length and resistance with a DC power supply of each specimen were measured. (3) The resistivity of each specimen was calculated according to formula (1), and the obtained resistivity was subsequently converted into conductivity. By comparing the conductivity values of five specimens, the uniform conductivity of each composite filament was characterized, and the effects of different CNT contents on the conductivity

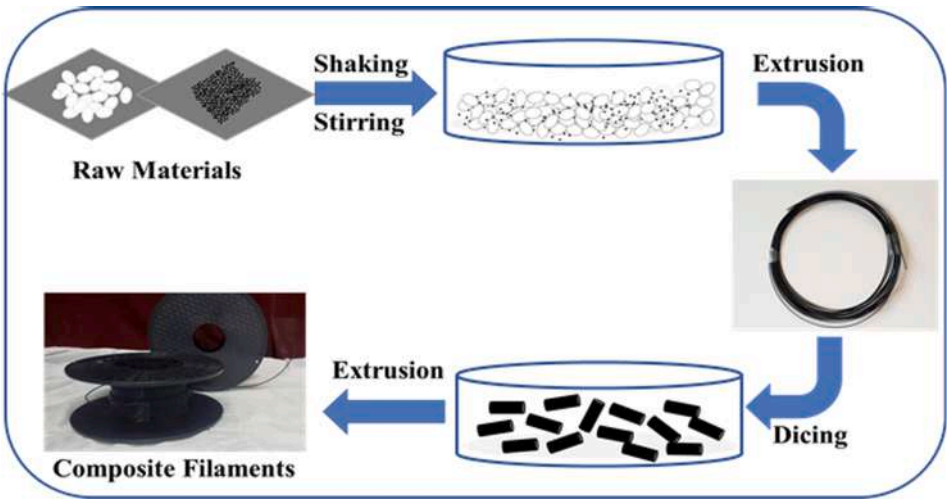

Fig. 1. Schematic for the preparation of PLA/CNT composite filaments.

of PLA/CNT composites were analyzed.

2.3.2. Thermal property measurement

Differential scanning calorimetry (DSC) was carried out on a Mettler-Toledo DSC 1 STAR SYSTEM to characterize the thermal properties of the samples. The samples were heated from 25 °C to 200 °C and then cooled to room temperature at a rate of 5 °C/min for two consecutive cycles. The data of the second heating process was selected to eliminate the influence of thermal history.

Thermogravimetric analyses (TGA) were executed on a METTLER TOLEDO TGA/DSC 1 thermogravimetric analyzer. The samples were heated from room temperature to 700 °C at a rate of 10 °C /min in a nitrogen atmosphere under a gas flow rate of 40 ml/min.

2.3.3. Dynamic mechanical analysis

Dynamic mechanical analyses (DMA) were performed on a TA Q800 instrument under the tension mode. The samples were heated from 20 °C to 130 °C at a heating rate of 5 °C/min, a frequency of 1 Hz and amplitude of 20 μm. PLA and PLA/CNT composite filaments were cut into pieces of 30 mm in length.

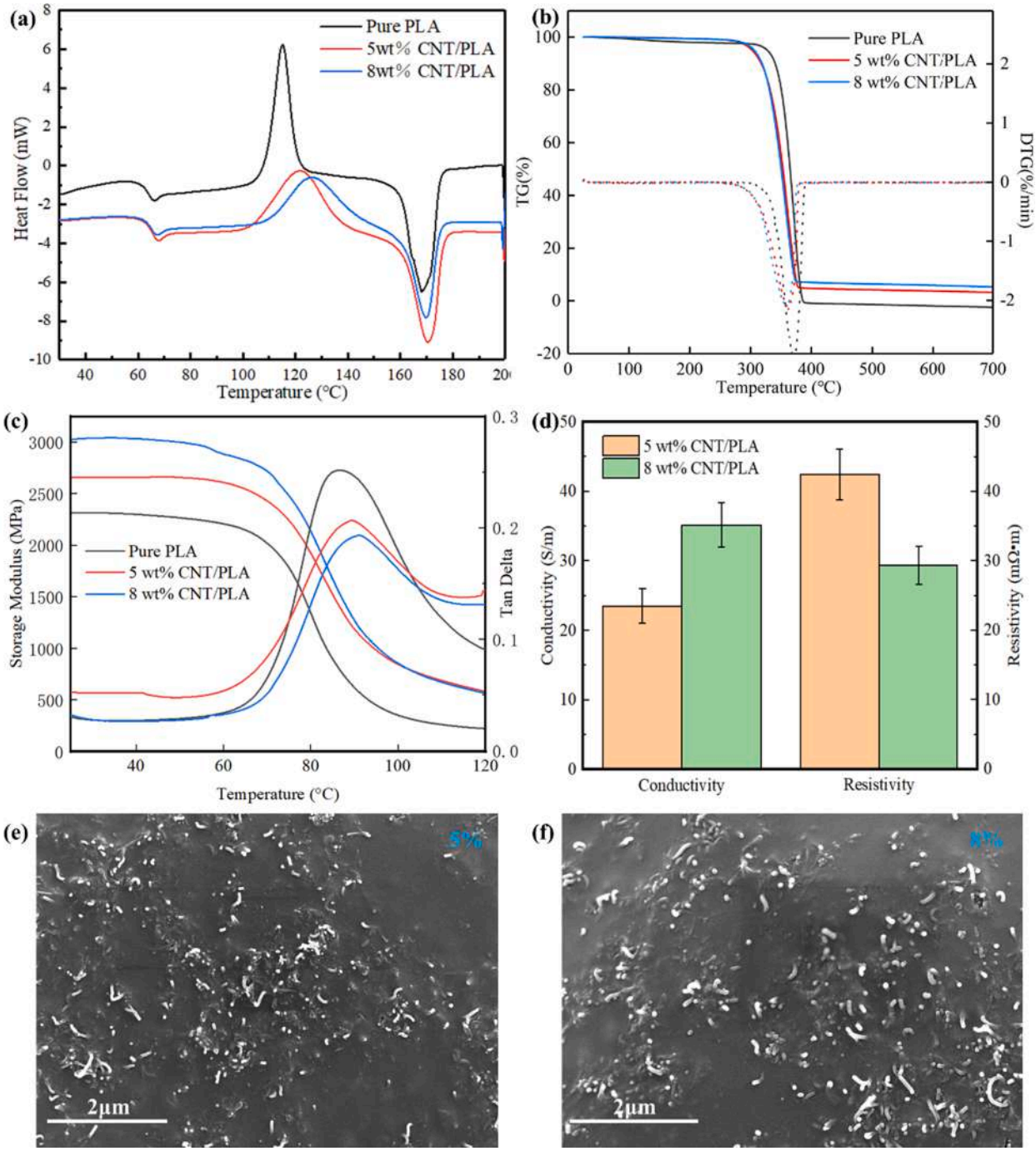

Fig. 2. (a) DSC curves of PLA/CNT electro-active SMPC specimens, (b) TGA curves of SMPC specimens, (c) DMA curves of SMPC specimens, (d) Conductivity test results of filaments, (e) SEM image of the cross-section of PLA/CNT filament with 5 wt% CNT, and (f) SEM image of the cross-section of PLA/CNT filament with 8 wt % CNT.

2.4. Electroactive shape memory behavior

The shape memory performances of the filaments and the 4D printed structures were tested by a DC power (ITECH IT6154) and an infrared camera (JENOPTIK InfraTec). Electrodes of the power supply were connected to the opposite ends of each filament specimen or the presetting energization position of each printed structure to ensure overall conduction. The applied voltage was adjusted to the appropriate value of U_r to ensure that each specimen was just heated above its T_g. The shape memory behaviors were examined by a bending test using rectangular strip specimens as the permanent shape. An external force was then applied to deform each specimen to the presetting deformation state (U shape) at 70 °C, and the force was maintained after turning off the power until the specimen became cooled and hardened, which is named as shape fixing process. The voltage U_r was then again applied to the specimen, and the time to reach the maximum recovery (T_r), θ_s is the sagging angle when the external force is removed in the cold; θ_r is the shape recovery angle in the shape recovery process. The shape fixity ratio (R_f) shape recovery rate (R_r) was calculated according to the following formulas (a) and (3) [41].

$$R_f = \frac{180^\circ - \theta_s}{180^\circ} \times 100\% \quad (2)$$

$$R_r = \frac{\theta_r}{180^\circ - \theta_s} \times 100\% \quad (3)$$

3. Results and discussion

3.1. Basic properties of composites

Fig. 2a presents the DSC results of PLA filaments PLA/CNT composite filaments (5 wt% and 8 wt%). The T_g of PLA was around 66 °C, and the addition of CNTs slightly increased the T_g of the composites. The crystal peak of PLA was noticed at 115 °C, whereas those for 5 wt% and 8 wt% PLA/CNT composite filaments were detected at 121 °C and 126 °C, respectively. It happened because CNTs acted as heterogeneous nucleation points to increase the crystallization temperature of the PLA matrix. The melting temperatures of these three specimens were about the same, and the endothermic peak was around 170 °C. The shape memory effect of printed structures can only be noticed between T_g and T_m; therefore, the working temperature of these structures should be controlled within this temperature range. Moreover, during 4D printing, the printing temperature should be 20–40 °C higher than T_m to prevent nozzle clogging.

The TGA curves of PLA filaments and PLA/CNT composite filaments (5 wt% and 8 wt%) are exhibited in Fig. 2b. The decomposition temperature of pure PLA started at 313.5 °C and ended at 389 °C. The decomposition temperature of the 5 wt% CNT-filled filament started at 274.8 °C and ended at 379.6 °C, whereas the decomposition temperature of the 8 wt% CNT-filled filament started at 269.9 °C and ended at 375.7 °C. It can be seen from the TGA results that the thermal decomposition temperature of the filaments decreased with the increase of CNT contents. In addition, the remaining mass of the PLA/ CNT filaments of 5 wt% and 8 wt% was almost unchanged around 600 °C and the weight fraction of CNT in the filament was around 5% and 8%, which was consistent with the proportion of the experimental design.

The DMA curves (storage modulus versus temperature) of pure PLA, 5 wt% and 8 wt% PLA/CNT filaments are exhibited in Fig. 2c. The storage modulus of 5 wt% and 8 wt% PLA/CNT was much higher than that of pure PLA because the addition of CNTs significantly enhanced the stiffness of the PLA matrix. The T_g values of pure PLA, 5 wt% and 8 wt% PLA/CNT were around 90 °C, higher than DSC results due to the different test mechanisms. With the increase of CNT contents, the T_g of PLA/CNT increased. This trend is consistent with DSC results.

For each filament, the conductivity and resistivity of PLA/CNT SMPC filaments (5 wt% and 8 wt%) were tested at five different parts and the average value was calculated. Fig. 2d presents the conductivity and resistivity of PLA/CNT SMPC filaments (5 wt% and 8 wt%). Both filaments had considerable conductivity, and 8 wt% PLA/CNT had a significantly higher value. It can be attributed to the higher forming possibility of a continuous conductive network inside the SMPC with the increase of the CNT content. Compared to the pure PLA, the electrical conductivity and thermal conductivity of the pure PLA were enhanced after the addition of CNT (Fig. 2d and Table. S1). In order to demonstrate the PLA/CNT composite filament with uniform particle distribution, SEM was carried out to test the cross-section of the composite filament. From SEM images of PLA/CNT composite filament, as shown in Fig. 2e and Fig. 2f, we can see CNTs are distributed uniformly in the PLA matric, which is significant for the conductivity property.

3.2. Electroactive shape memory performance of composite filaments

Both 5 wt% and 8 wt% PLA/CNT filaments were bent into a U-shape to test their electroactive shape memory performance. The corresponding test results are shown in Table. 1, and the electroactive shape recovery processes of both specimens are displayed in Fig. 3. Although the lengths of the two specimens were similar, the electroactive shape memory performance of the 8 wt% specimen was superior to that of the 5 wt% composite filament. It happened because adding a higher CNT content significantly improved the electrical conductivity and thermal conductivity of the 8 wt% composite filament. Compared to the 8 wt% specimen, the 5 wt% composite filament had lower heat production efficiency and poorer heat conductivity, resulting in uneven heat distribution in different parts of the specimen and an unsatisfying shape recovery performance. Hence, 8 wt% composite filaments were used to fabricate printed structures.

3.3. Electroactive shape memory performance of 4D printed film structures

In comparison to filaments, factors affecting the electroactive shape memory performance of printed structures are more complicated. In order to explore the influences of different printing parameters on the shape memory performance of printed structures, strip-shaped (Fig. 4a) and U-shaped (Fig. 4b) structures are designed. These two structures had a thickness of 0.6 mm and included three identical single layers; thus, they could be regarded as two-dimensional structures. The interior filling method of the strip-shaped structure was linear, and filling wires were placed parallel to the axial direction. Electrodes were connected at both ends of the structure to make it energized and heated. An infrared camera was used to observe the heating process of the structure (Fig. 4a). Due to the good electrical conductivity and thermal conductivity of the printed structures (Table. S2), the internal heat distribution and heating rate were very uniform, indicating that the electrical conductivity of the structure did not change significantly along the direction of internal filling wires. The printing process has little effect on the thermal properties of the printed structures (Fig. S1a). However, the storage modulus of the printed structures decreased slightly (Fig. S1b), the reason may be that the printing structure was formed by melt printing layer by layer, with a small number of voids, which is not dense, resulting in the reduction of storage modulus.

The printed U-shaped structure shown in Fig. 4b was used to test the influences of different internal filling wires with direction on its shape

Table 1
Electroactive shape memory testing results of PLA/CNT filament specimens.

Samples	5% CNT	8% CNT
Driving voltage (v)	20	10
Recovery time (s)	90	30
Shape recovery ratio (%)	80	100

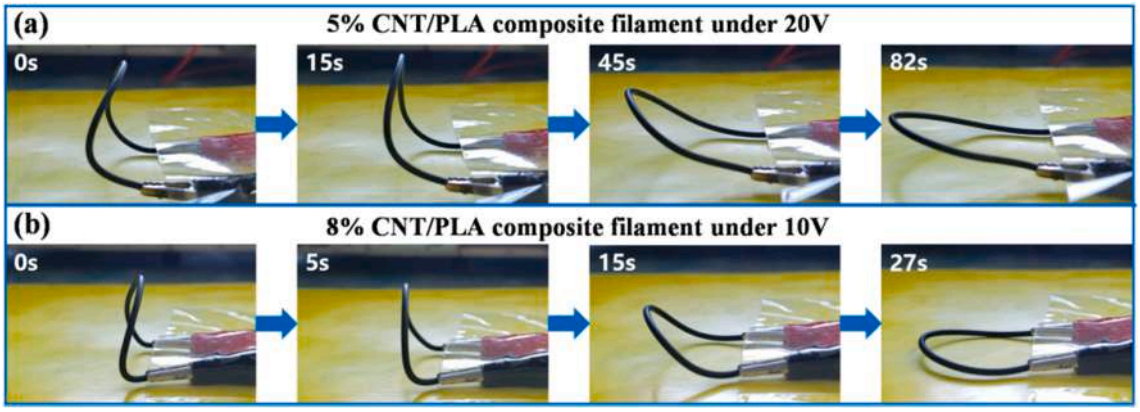

Fig. 3. Electroactive shape recovery process of SMPC filament: (a) 5 wt% PLA/CNT and (b) PLA/CNT 8 wt%.

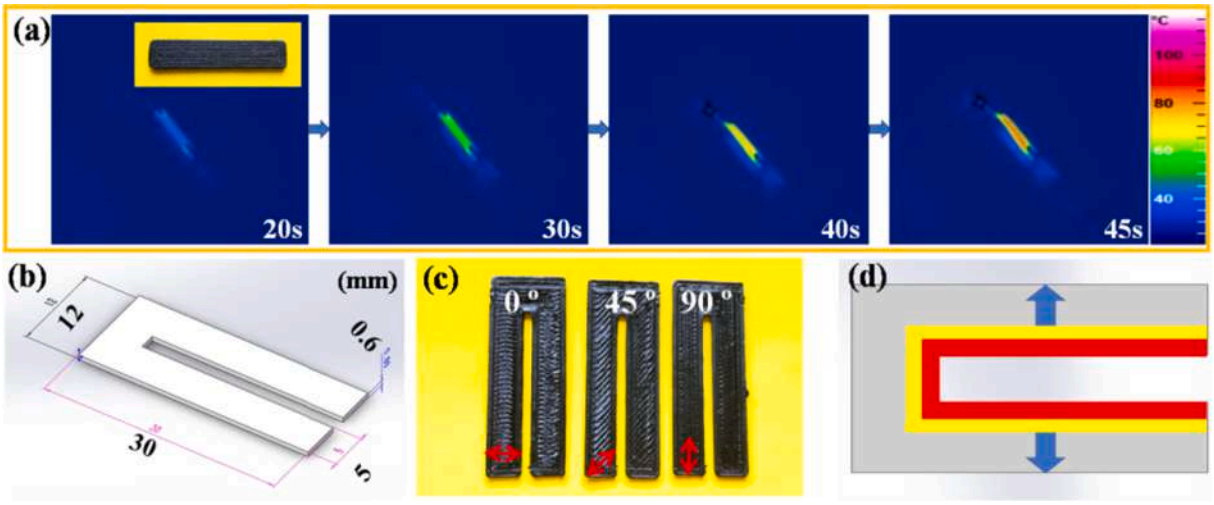

Fig. 4. 2D printed structures: (a) heat distribution of the strip-shaped structure during the energization process, (b) U-shaped structure, (c) U-shaped structure with different infill directions (0°, 45°, 90°), and (d) heat diffusion direction inside the U-shaped structure.

memory performance. A total of three U-shaped structures with different filling directions (0°, 45°, 90°) were prepared (Fig. 4c). The U-shaped structure bent in the perpendicular direction to the board surface, and the two long legs of the structure were the main deformation parts. Theoretically, when electrodes were connected at the edge of the two long legs of the U-shaped structure, and overall energization could be realized; however, in the actual scenario, the current mainly passed through the innermost part of the structure with the shortest total distance and the temperature rise in other parts mainly depended on heat diffusion from this area; hence, the thermal conductivity of the structure along the direction perpendicular to the two long legs as shown in Fig. 4d had a significant impact on the shape memory behavior. The electroactive shape memory performances of three different types of U-shaped structures are shown in Table. 2. For the programming process, the voltage was adjusted to make the current in each branch of the printed sample the same (the current of each branch was controlled at about 0.1A) to keep the component programming temperature consistent. The electroactive shape recovery processes are displayed in Fig. 5, and their internal heat distribution image are presented in Fig. 6.

Table 2
Electroactive shape memory test results of U-shaped structures with three different filling directions.

Filling Direction	0°	45°	90°
Activation Voltage (v)	35	45	50
Recovery Time span (s)	80	70	90
Shape Recovery Ratio (%)	83.3	98	95
Shape Fixation Ratio (%)	100	100	100

The specimen with 0° infill direction had the most uniform internal heat distribution and the lowest activation voltage. In contrast, the specimen with 90° infill direction had the worst internal heat distribution uniformity and the highest activation voltage. This difference can be attributed to the filling directions of the structures. The deformation of the U-shaped structure mainly occurred in its two long legs. Interior filling wires of the 0° specimen were parallel to the heat transfer direction in two legs of the structure, whereas filling wires of the 90° specimen were parallel to the direction of two legs of the structure. The Joule heat of the former type was quickly transferred to other areas of the structure through interior filling wires, whereas the latter type needed to transfer heat through contacts between different filling wires, resulting in a large thermal conductivity difference. On the contrary, the final shape recovery ratio of the 0° specimen was the lowest (less than 90%), whereas that of the 90° specimen could reach 95%. As the filling direction was perpendicular to two legs of the 0° specimen, only filling wires of the bent part were deformed during the deformation process. Hence, only these filling wires participated in the shape recovery process when the specimen was energized again; thus, the shape recovery force was significantly low. By contrast, interior filling wires of the 90° specimen were parallel to the two-leg direction; thus, almost all filling wires became bent during the deformation process. Only a small part of the structure reached above T_g during the initial stage of energization,

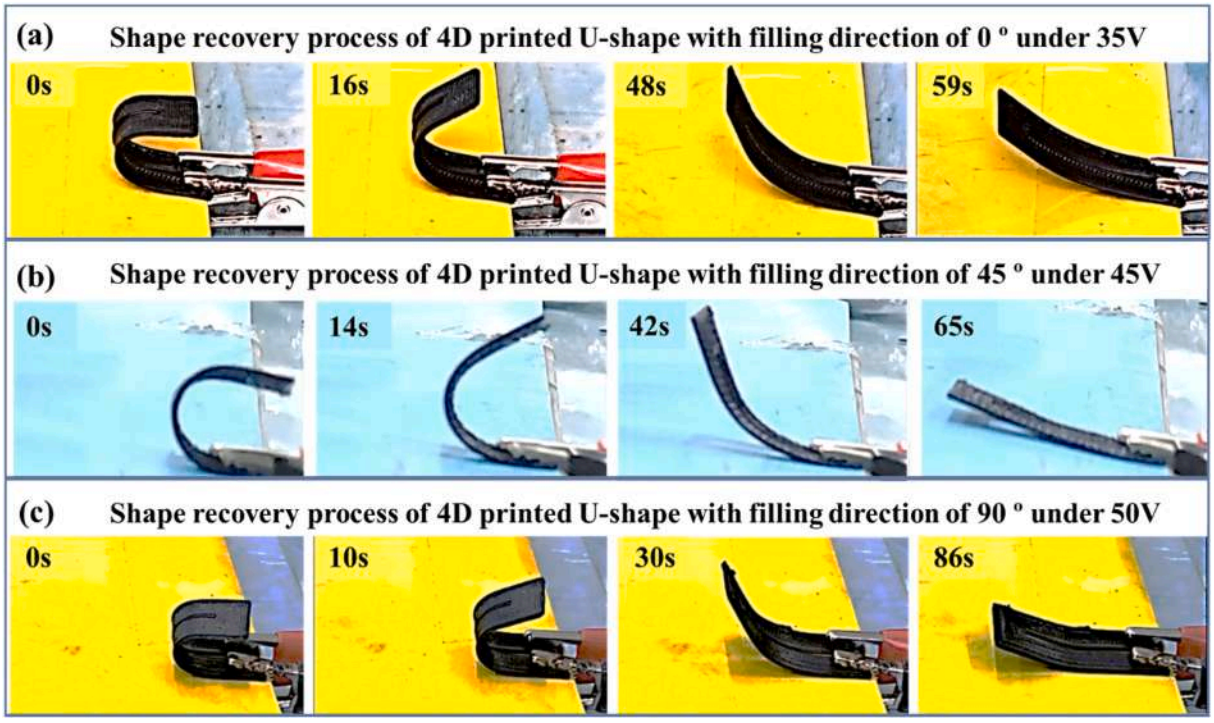

Fig. 5. Electroactive shape recovery processes of U-shaped structures: (a) 0° infill direction, (b) 45° infill direction, and (c) 90° infill direction.

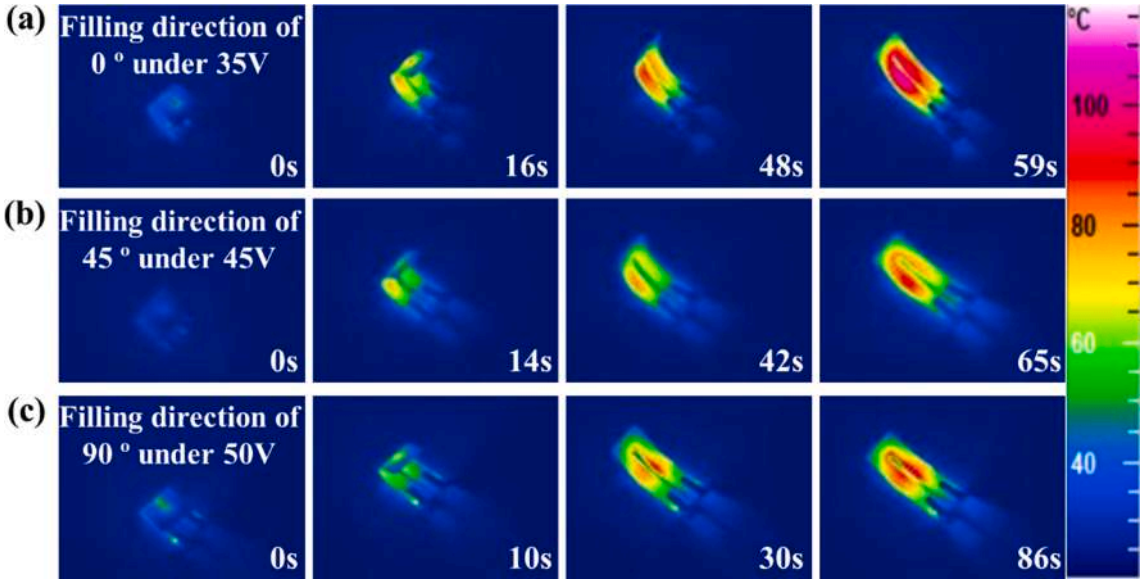

Fig. 6. Heat distribution maps of U-shaped structures: (a) 0° infill direction, (b) 45° infill direction, and (c) 90° infill direction during the electroactive shape recovery process.

and the rest could not be softened, resulting in a large deformation resistance. The 45° specimen manifested a more comprehensive performance, balanced thermal conductivity, and had the shortest recovery time and the highest shape recovery ratio.

3.4. Electroactive shape memory performance of 4D printed composite structures

As 3D structures require more printing layers and their circuit design is far more complicated than 2D ones, their performance is subjected to more factors. As the current mainly flows along the shortest path inside a printed structure, 3D structures need an extremely high heating power. Under the consideration of driving efficiency, a 3D electroactive structure consisting of several shunt branches was designed as the frame structure. In addition, in order to ensure that the entire structure had the same heating efficiency, branches with the same voltage at both ends were designed to have the same resistance and thermal conductivity; hence, each branch connected to the same power source should have the same length. Moreover, the layer-by-layer forming characteristics of FDM made each branch have a different internal structure, resulting in different heating efficiencies.

In order to determine this effect, a pyramid-shaped structure with three equal-length branches was designed as shown in Fig. 7a. Under two different printing directions (Fig. 7b and Fig. 7c), a type-A specimen

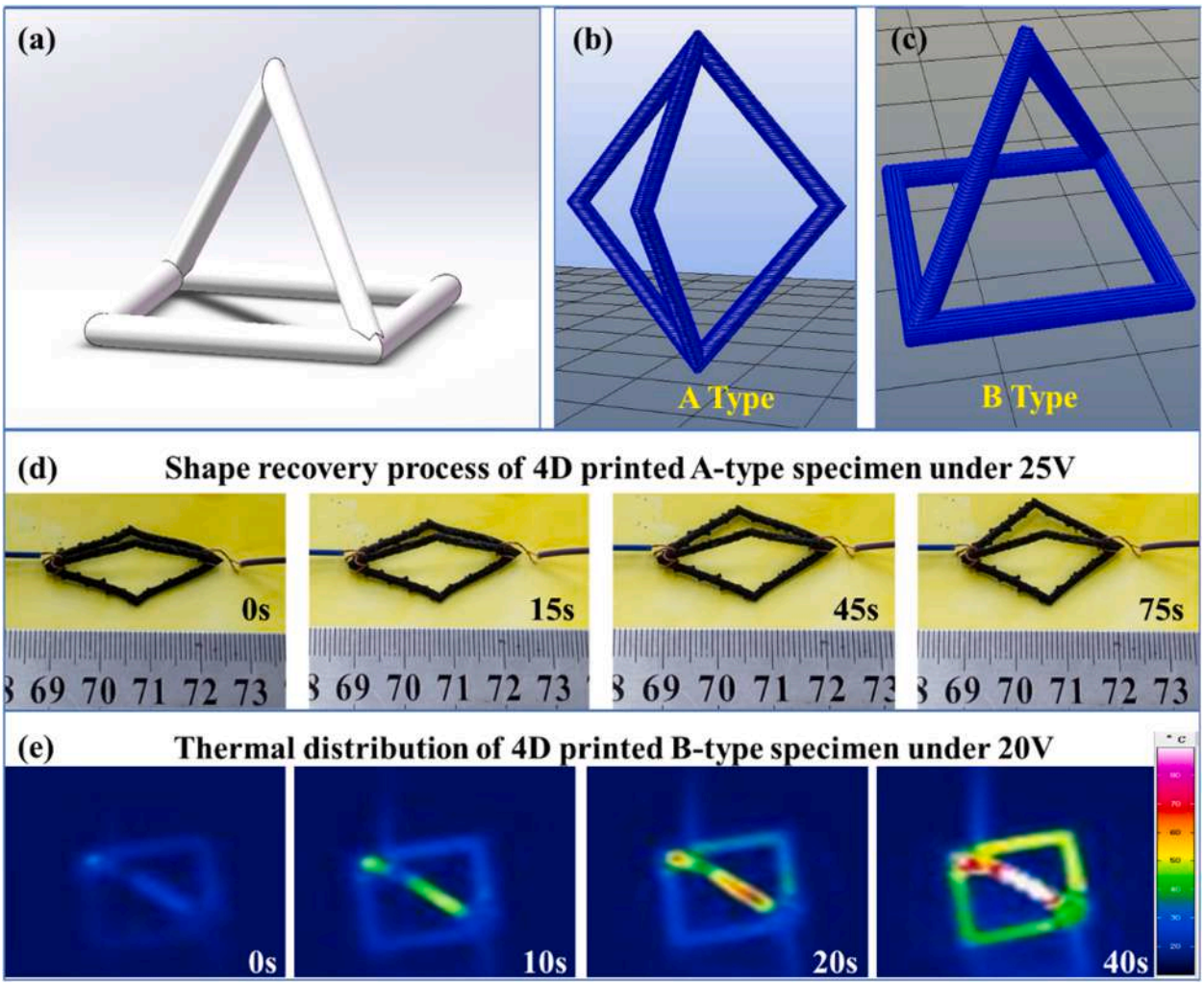

Fig. 7. 4D printed electroactive pyramid-shaped structure. (a) model of pyramid-shaped structure; (b) printing direction of the type-A specimen which contains three branches of identical infill structure; (c) printing direction of the type-B specimen including three branches of two kinds of infill structure; (d) Electroactive shape recovery process of the type-A specimen and (e) heat distribution of the type-B specimen during energization process.

with three branches of the same internal structure and a type-B specimen with three branches of two different internal structures were prepared. These two specimens were energized and elongated and then subjected to an electroactive shape memory test. The electroactive shape memory recovery process of the type-A specimen is displayed in Fig. 7d. The three branches of the specimen had the same heating efficiency, their deformations were synchronized during the entire energization process, and the original shape was completely recovered within 75 s. The type-B specimen, after being energized, manifested no shape memory behavior (Fig. 7e), and its equal-length branches with different internal structures had different heating efficiencies. It was found that the branch parallel to the direction of the current was always preferentially heated. The low printing accuracy led to insufficient contact quality between filling wires in the structure, and in the stacking direction, structure layers were in closer contact by gravity, resulting in better conductivity. The programming temperature was 70 °C. The shape fixity of the sample was about 100%. The recovery temperature was around 70 °C. Hence, in the design process of 4D printed electroactive structures, in addition to improving the printing accuracy, it is necessary to ensure that branches participating in deformation have the same internal printing structure.

Furthermore, a diamond-shaped structure (Fig. 8a) is also designed. After connecting them to a power supply, they had 12 and 8 branches of the same length, respectively. These branches were composed of oblique edges, and no current flowed in horizontal edges. The diamond-shaped structure exhibited excellent electroactive shape memory performance. After being compressed, it could completely recover to its original shape within 23 s (Fig. 8b). And the thermal distribution of the diamond-shaped structure is shown in Fig. 8c. Moreover, a crown-shaped structure as shown in Fig. 8d is designed. By contrast, the shape memory performance of the crown-shaped structure was weaker. After its eight-pointed ends became bent, it took 44 s to achieve a 75% shape recovery ratio (Fig. 8e). The thermal distribution of the diamond-shaped structure is shown in Fig. 8f. Therefore, it can be inferred that the shape memory performance of 4D printed structures mainly depends on their shape recovery force. Each branch of the diamond-shaped structure worked synchronously to produce a greater recovery force. The deformation degree of each branch of the diamond-shaped structure was the same. The resulting conductivity change was also synchronized; hence, its eight branches had the same shape recovery degree during the re-energization process. By contrast, each branch of the crown-shaped structure deformed independently. The conductivity change of each branch was different during the shape recovery process; hence, the heating conditions of each branch were different, resulting in poor electroactive shape memory recovery performance.

Furthermore, two 4D printed electroactive SMPC structures with practical application potentials were designed. The first one was a multi-segment controllable actuator that could be deployed in three states, as shown in Fig. 9a. The actuator was composed of three identical

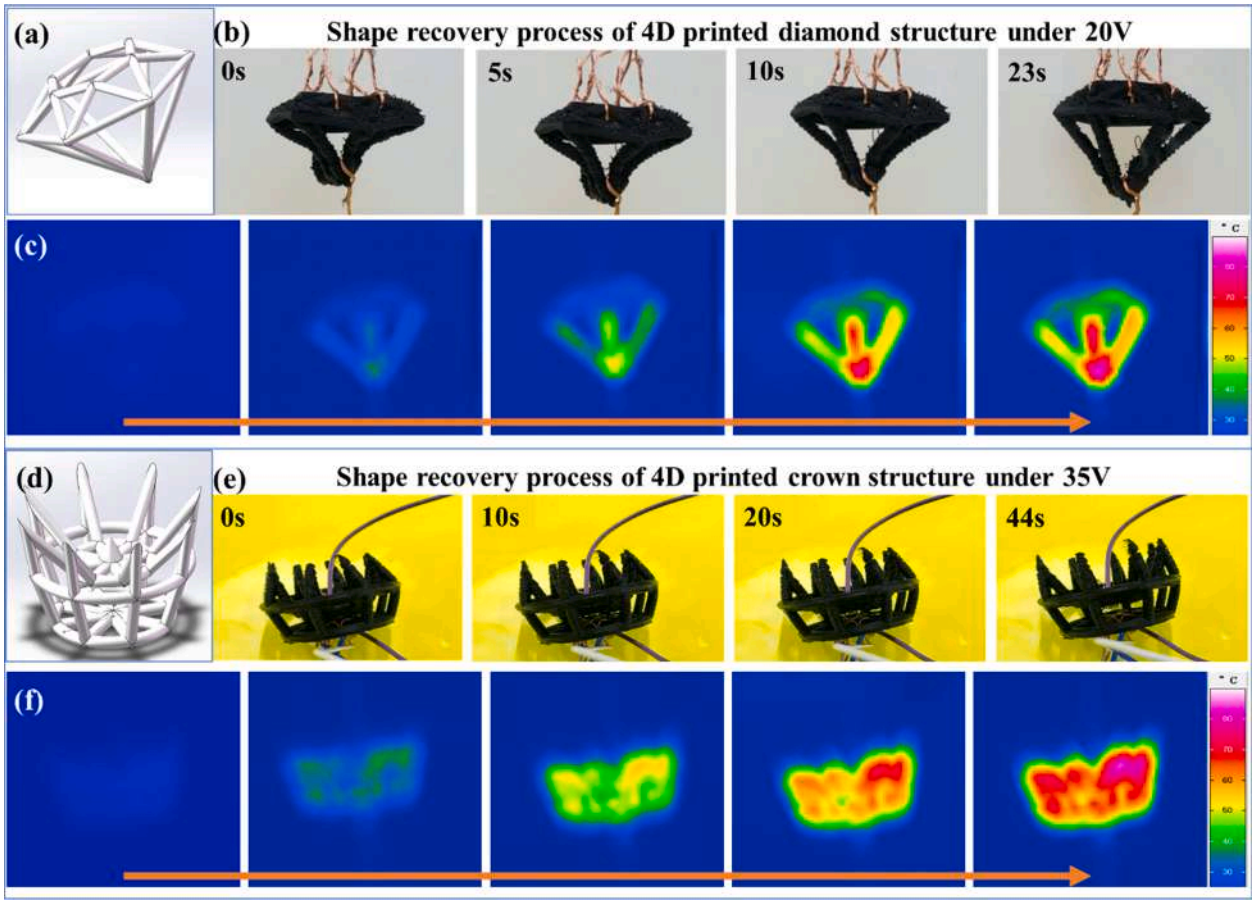

Fig. 8. Diamond-shaped and crown-shaped structures: (a) model of the diamond-shaped structure, (b) electroactive shape recovery process of the diamond-shaped structure, (c) heating process of diamond, (d) model of the crown-shaped structure, (e) electroactive shape recovery process of the crown-shaped structure, and (f) heating process of crown.

rectangular parallelepiped frames that were fixed in a bent state. Connecting the actuator to a power supply according to the connection methods I-III shown in Fig. 9b-d, the deformations of segments 1–3 of the device corresponding to the 1–3 deployment states could be controlled. The bent and level 1–3 deployment states of the actuator at 25 V (around 70 °C) are shown in Fig. 9e-h. The actuation of the multi-segment controllable actuator at different segments can be controlled and designed (Fig. S2). Compared to actuators based on motors or artificial muscles, this SMPC actuator had a more straightforward principle and manufacturing process, lighter weight, and lower cost; however, it had some significant problems of low control accuracy and small driving force.

The second structure was an external fixation stent as shown in Fig. 10a. The stent had a net structure composed of diamond-shaped grids and was initially in a curled state. The stent became energized and heated when electrodes were connected at vertices of the top and bottom grids. The stent was unfolded before use and then placed outside the body part that needed to be fixed. The stent automatically shrank after being energized and exhibited a good holding and fixing effect after cooling. The clamping process of the stent under energization at 20 V is shown in Fig. 10b, and it completed 90% of shape recovery within 60 s. This external fixation stent was easy and quick to operate and had an excellent fixing effect.

4. Conclusions

A facile method to fabricate electroactive shape memory structures by FDM was proposed in the current research. First, a commercial FDM printing standard filament was prepared using PLA/CNT SMPC as the raw materials by successfully combining the electrical conductivity of CNTs with the shape memory effect of PLA. The electrical, thermal, and electroactive shape memory properties of the filament were characterized. With the increase of the CNT content within a certain range, the electrical conductivity, thermal conductivity, and shape recovery ratio of SMPC manifested an upward trend. Subsequently, a series of 2D and 3D structures were printed with the abovementioned filament and their electroactive shape memory cycles were realized. In addition, by changing printing parameter settings and structures, the influencing factors for the electroactive shape memory performance of the 4D-printed SMPC structures were investigated, and the resultant structures manifested excellent electroactive shape memory performance. The shape fixation ratio was 100% at room temperature, whereas the shape recovery ratio reached more than 90% under a certain voltage. Finally, two electroactive deformable devices with certain application potentials were designed and prepared based on the abovementioned method. This work broadens the range of potential materials in the 4D printing field and provides a new forming route for electroactive SMPC.

CRediT authorship contribution statement

Xinyu Dong: Investigation, Validation, Formal analysis, Data curation, Writing – original draft. **Fenghua Zhang:** Conceptualization, Methodology, Formal analysis, Resources, Writing – original draft, Writing – review & editing, Supervision, Project administration, Funding acquisition. **Linlin Wang:** Formal analysis, Investigation. **Yanju Liu:** Resources, Funding acquisition. **Jinsong Leng:** Resources, Project administration, Supervision, Funding acquisition.

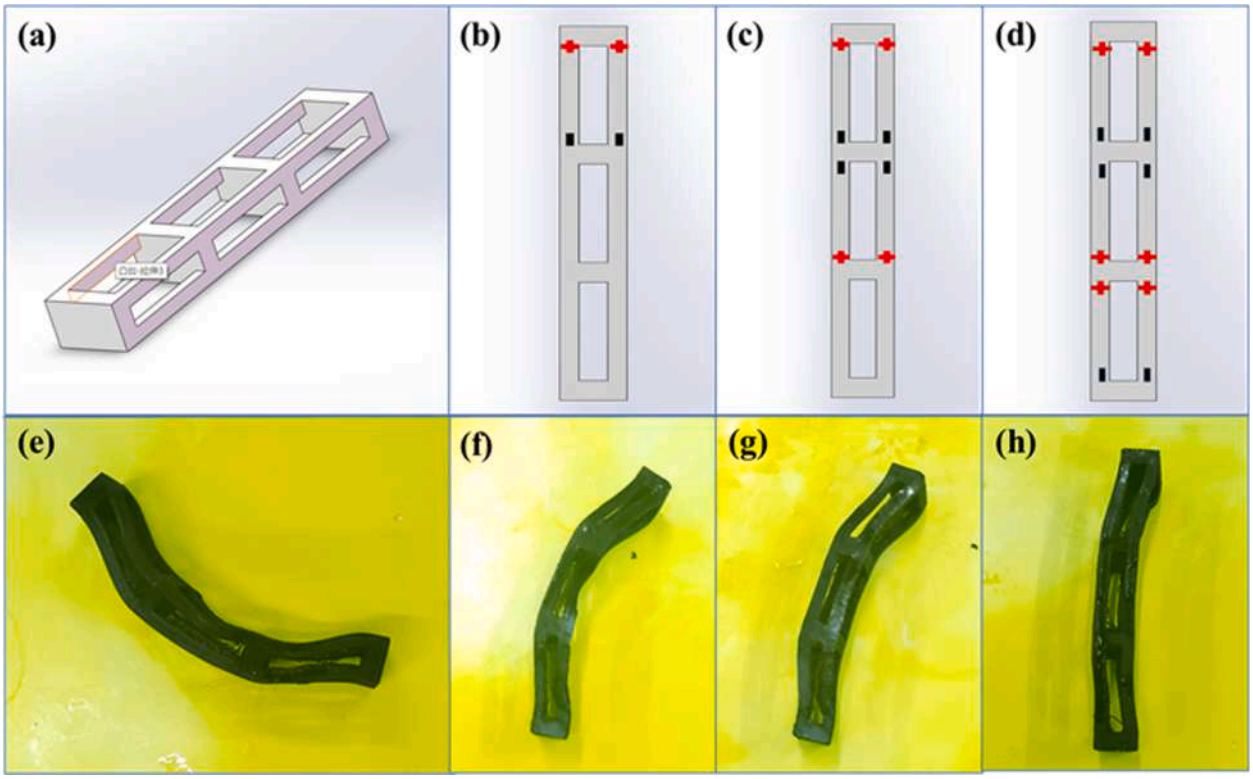

Fig. 9. 4D printed electroactive multi-segment controllable actuator at 25 V: (a) model of the actuator, (b) connecting method I corresponding to segment 1 control, (c) connecting method II corresponding to segments 2 control, (d) connecting method III corresponding to segments 3 control, (e) actuator in the bent state, (f) actuator in the level 1 deployment state, (g) actuator in the level 2 deployment state, and (h) actuator in the level 3 deployment state.

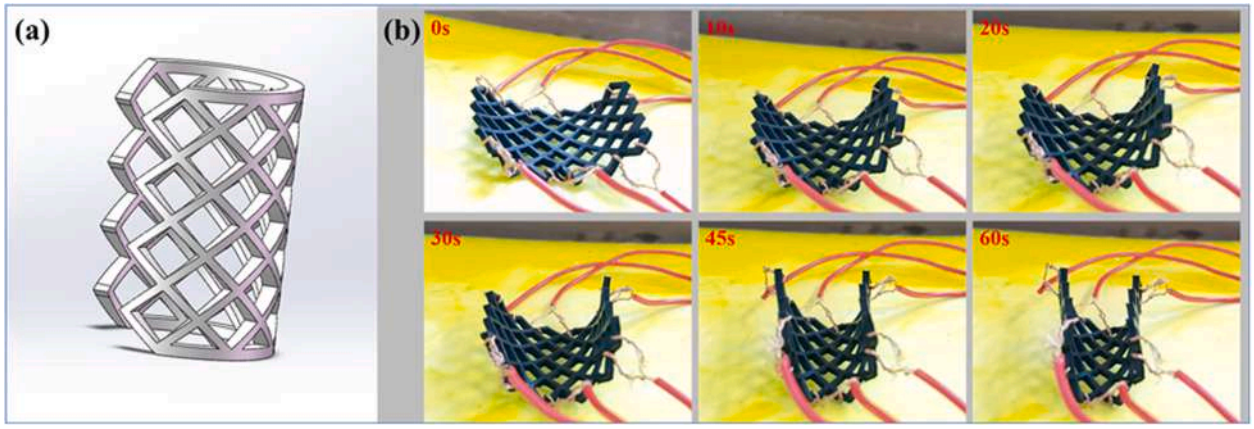

Fig. 10. 4D printed electroactive external fixation stent: (a) model of the external fixation stent and (b) electroactive clamping process.

Declaration of Competing Interest

The authors declare that they have no known competing financial interests or personal relationships that could have appeared to influence the work reported in this paper.

Acknowledgments

This work is funded by the National Natural Science Foundation of China (Grant No.11632005, 11802075, 12072094). This work is also supported by the China Postdoctoral Science Foundation funded project.

Appendix A. Supplementary material

Supplementary data to this article can be found online at https://doi.org/10.1016/j.compositesa.2022.106925.

References

[1] Raviv D, Zhao W, McKnelly C, Papadopoulou A, Kadambi A, Shi B, et al. Active printed materials for complex self-evolving deformation. Sci Rep 2014;4(1):7422.
[2] Ge Q, Qi HJ, Dunn ML. Active materials by four-dimension printing. Appl Phys Lett. 2013;13:131901.
[3] Momeni F, Ni J. Laws of 4D printing. Engineering 2020;6(9):1035–55.
[4] Wang Y, Cui H, Wang Y, Xu C, Esworthy TJ, Hann SY, et al. 4D printed cardiac construct with aligned myofibers and adjustable curvature for myocardial regeneration. ACS Appl Mater Inter. 2021;13(11):12746–58. https://doi.org/10.1021/acsami.0c17610.

[5] Zhang W, Wang H, Wang H, Chan JYE, Liu H, Zhang B, et al. Structural multi-colour invisible inks with submicron 4D printing of shape memory polymers. Nat Commun 2021;12(1):112.
[6] Li YJ, Zhang FH, Liu YJ, Leng JS. 4D printed shape memory polymers and their structures for biomedical applications. Sci China Technol Sc 2020;63(4):545–60.
[7] Lin C, Liu L, Liu Y, Leng J. 4D printing of bioinspired absorbable left atrial appendage occluders: a proof-of-concept study. ACS Appl Mater Inter 2021;13(11):12668–78.
[8] Khoo ZX, Teoh JEM, Liu Y, et al. 3D printing of smart materials: a review on recent progresses in 4D printing. Virtual Phys Prototy 2015;3:103–22.
[9] Kim K, Zhu W, Qu X, et al. 3D optical printing of piezoelectric nanoparticle - polymer composite materials. ACS Nano 2014;10:9799–805.
[10] Dadbakhsh S, Speirs M, Kruth JP, et al. Effect of SLM parameters on transformation temperatures of shape memory nickel titanium parts. Adv Eng Mater 2014;9:1140–6.
[11] Lee AY, An J, Chua CK. Two-way 4D printing: a review on the reversibility of 3D-printed shape memory materials. Engineering 2017;3:663–74.
[12] Liu C, Qin H, Mather PT. Review of progress in shape-memory polymers. J Mater Chem 2007;16:1543–58.
[13] Behl M, Lendlein A. Shape-memory polymers. Mater Today 2007;10:20–8.
[14] Xia Y, He Y, Zhang F, Liu Y, Leng J. A review of shape memory polymers and composites: mechanisms, materials, and applications. Adv Mater 2021;33(6):2000713.
[15] Liu Y, Zhang F, Leng J, Chou T-W. Microstructural design of 4D printed angle-ply laminated strips with tunable shape memory properties. Mater Lett 2021;285:129197.
[16] Lendlein A, Jiang HY, Junger O, et al. Light-induced shape-memory polymers. Nature 2005;7035:879–82.
[17] Lu HB, Yao YT, Huang WM, et al. Significantly improving infrared light-induced shape recovery behavior of shape memory polymeric nanocomposite via a synergistic effect of carbon nanotube and boron nitride. Compos Part B-Eng 2014;62:256–61.
[18] Liu Y, Du H, Liu L, Leng J. Shape memory polymers and their composites in aerospace applications: a review. Smart Mater Struct 2014;23(2):023001.
[19] Lu H, Liu Y, Gou J, Leng J, Du S. Synergistic effect of carbon nanofiber and carbon nanopaper on shape memory polymer composite. Appl Phys Lett 2010;96(8):084102.
[20] Leng JS, Lan X, Liu YJ, et al. Shape-memory polymers and their composites: stimulus methods and applications. Prog Mater Sci 2011;7:1077–135.
[21] Buckley PR, Mckinley GH, Wilson TS, et al. Inductively heated shape memory polymer for the magnetic actuation of medical devices. IEEE T Bio-Med Eng 2006;53:2075–83.
[22] Wang W, Timonen JVI, Carlson A, Drotlef D-M, Zhang CT, Kolle S, et al. Multifunctional ferrofluid-infused surfaces with reconfigurable multiscale topography. Nature 2018;559(7712):77–82.
[23] Liu Y, Zhang W, Zhang F, Lan X, Leng J, Liu S, et al. Shape memory behavior and recovery force of 4D printed laminated Miura-origami structures subjected to compressive loading. Compos Part B-Eng 2018;153:233–42.
[24] Zhang W, Zhang F, Lan X, Leng J, Wu AS, Bryson TM, et al. Shape memory behavior and recovery force of 4D printed textile functional composites. Compos Sci Technol. 2018;160:224–30.
[25] Lee AY, An J, Chua CK, Zhang Yi. Preliminary investigation of the reversible 4D printing of a dual-layer component. Engineering 2019;5(6):1159–70.
[26] Meng H, Li GQ. A review of stimuli-responsive shape memory polymer composites. Polymer 2013;54:2199–221.
[27] Zhao W, Liu L, Zhang F, Leng J, Liu Y. Shape memory polymers and their composites in biomedical applications. Mar Sci Eng C-Mater 2019;97:864–83.
[28] Xie T. Tunable polymer multi-shape memory effect. Nature 2010;464:267–70.
[29] Chen L, Li W, Liu Y, Leng J. Nanocomposites of epoxy-based shape memory polymer and thermally reduced graphite oxide: mechanical, thermal and shape memory characterizations. Compos Part B-Eng 2016;91:75–82.
[30] Wang Y, Ma T, Tian W, Ye J, Wang X, Jiang X. Electroactive shape memory properties of graphene/epoxy-cyanate ester nanocomposites. Pigm Resin Technol 2018;47(1):72–8.
[31] Wang Y, Ye J, Tian W. Shape memory polymer composites of poly(styrene-b-butadiene-b-styrene) copolymer/liner low density polyethylene/Fe_3O_4 nanoparticles for remote activation. Appl Sci-Basel 2016;6(11):333.
[32] Kuang W, Mather PT. A latent crosslinkable PCL-based polyurethane: synthesis, shape memory, and enzymatic degradation. J Mater Res 2018;33(17):2463–76.
[33] Zhang F, Xia Y, Wang L, Liu L, Liu Y, Leng J. Conductive shape memory microfiber membranes with core−shell structures and electroactive performance. ACS Appl Mater Inter. 2018;10(41):35526–32.
[34] Liu W, Chen H, Ge M, Ni Q-Q, Gao Q. Electroactive shape memory composites with TiO_2 whiskers for switching an electrical circuit. Mater Design 2018;143:196–203.
[35] Cho JW, Kim JW, Jung YC, et al. Electroactive shape-memory polyurethane composites incorporating carbon nanotubes. Macromol Rapid Comm 2005;26:412–6.
[36] Li M, Chen J, Shi MT, et al. Electroactive anti-oxidant polyurethane elastomers with shape memory property as non-adherent wound dressing to enhance wound healing. Chem Eng J 2019;375:121999.
[37] Wang X, Sparkman J, Gou J. Electrical actuation and shape memory behavior of polyurethane composites incorporated with printed carbon nanotube layers. Compos Sci Technol 2017;141:8–15.
[38] Zhang F, Zhang Z, Liu Y, Leng J. Electrospun nanofiber membranes for electrically activated shape memory nanocomposites. Smart Mater Struct 2014;23(6):065020.
[39] Ge Q, Sakhael AH, Lee H, et al. Multimaterial 4D printing with tailorable shape memory polymers. Sci Rep 2016;6:31110.
[40] Wei H, Cauchy X, Navas IO, Abderrafai Y, Chizari K, Sundararaj U, et al. Direct 3D printing of hybrid nanofiber-based nanocomposites for highly conductive and shape memory applications. ACS Appl Mater Inter 2019;11(27):24523–32.
[41] Wan X, Zhang F, Liu Y, Leng J. CNT-based electro-responsive shape memory functionalized 3D printed nanocomposites for liquid sensors. Carbon 2019;155:77–87.
[42] Bodkhe S, Ermanni P. 3D printing of multifunctional materials for sensing and actuation: merging piezoelectricity with shape memory. Eur Polym J 2020;132:109738.
[43] Liu Y, Zhang W, Zhang F, Leng J, Pei S, Wang L, et al. Microstructural design for enhanced shape memory behavior of 4D printed composites based on carbon nanotube/polylactic acid filament. Compos Sci Technol 2019;181:107692.
[44] Mousavi S, Howard D, Zhang F, Leng J, Wang CH. Direct 3D printing of highly anisotropic, flexible, constriction-resistive sensors for multidirectional proprioception in soft robots. ACS Appl Mater Inter 2020;12(13):15631–43.
[45] Rosales CAG, Duarte MFG, Kim H, et al. 3D printing of shape memory polymer (SMP)/carbon black (CB). Mater Res Express 2018;5:065704.